

Restoration of continuous turbulence profile from lunar scintillation

A. Tokovinin

Version 1.1. June 11, 2008 [prj/atm/moon/doc/restor3.tex]

1 Introduction

Optical turbulence near the ground can be measured by a suitable analysis of lunar or solar scintillation. However, the problem of restoring the turbulence profile (TP) $C_n^2(h)$ from the covariances of intensity fluctuations in an array of detectors is non-trivial.

A simple and robust technique has been proposed [5] where linear combinations of the covariances are used to derive the turbulence integrals in a number of “layers”. Each layer is characterized by its own response function $\mathcal{R}(z)$, so the results are integrals $J = \int C_n^2(z)\mathcal{R}(z) dz$. The disadvantage of this method is that the response functions are quite wide (FWHM $\Delta z/z \sim 4$ for a 4-element array) and are defined along the line-of-sight $z = h \sec \gamma$ for altitude h and zenith distance γ . The interpretation of the results in terms of profile or its products such as integral in a given altitude range is problematic. For the same reason there is no straightforward way to get rid of the zenith-angle dependence.

Here we study the methods to derive a continuous $C_n^2(z)$ profile from the scintillometer data. Such methods were successfully used in the SHABAR restoration [3, 1]. The profile is defined by its values at certain fixed points – *pivot points*, and is interpolated between those points. As a first step, we use linear interpolation. This is equivalent to the de-composition of $C_n^2(z)$ on a set of triangular functions with vertices at the pivot points. Such linear restoration can be done very rapidly, in one step. However, the representation of $C_n^2(z)$ is necessarily very coarse. At the second step, we refine the result by using non-linear fitting of a more complex model which ensures the non-negativity of the C_n^2 .

Representing a continuous unknown TP by a coarse model with a few parameters is a kind of regularization necessary to solve the inverse problem. One does not expect a miracle, i.e. that the model would give an accurate representation of any profile. Instead, we hope that the model will render correctly the total intensity of the ground-layer turbulence and its location or thickness, therefore we test the accuracy of these parameters. In fact, the experience of the ATST site testing with SHABAR [3] shows that individual TPs are not very useful, as they contain excessive information. What is really needed usually is the measurement of the ground-layer seeing at few selected altitudes.

Table 1: Notation

Parameter	Notation	Dimension	Units
Range z and altitude h	$z = h \sec \gamma$	N_z	m
Turbulence profile	C_n^2, C	N_z	$\text{m}^{-2/3}$
Turbulence integrals	J	N_z or other	$\text{m}^{1/3}$
Covariance	B	N_b	—
Weight	W	$N_b \times N_z$	$\text{m}^{-1/3}$
Parameters	X	N_x	$\text{m}^{-2/3}$
Interaction matrix	A	$N_b \times N_x$	$\text{m}^{2/3}$
Triangular functions	T	$N_z \times N_x$	—

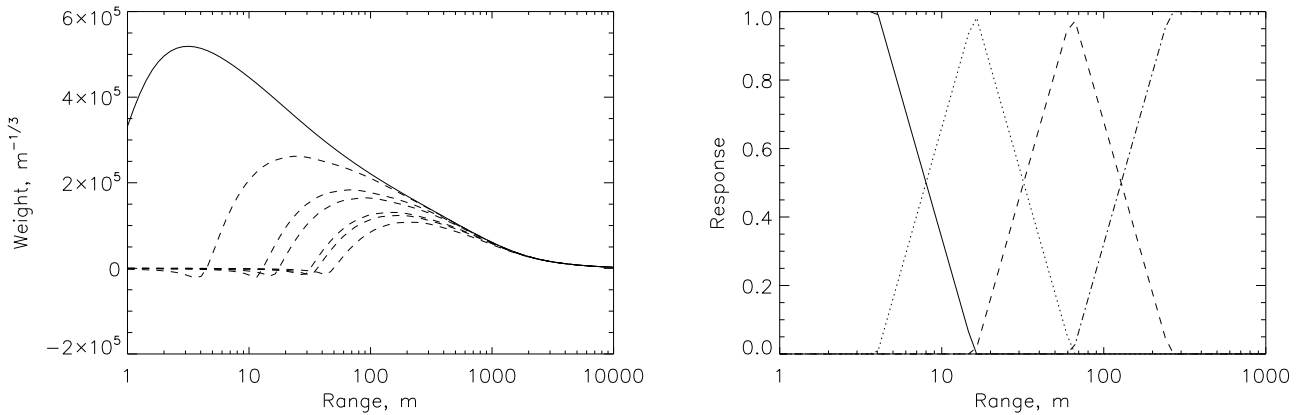


Figure 1: Left: Weighting function for the 4-element scintillometer array (full Moon). Right: triangular functions $T(z)$. [weight1,triang]

2 Restoration algorithm

2.1 Parameters and main relations

The covariance of intensity fluctuations B between two detectors separated by a baseline b depends on the turbulence distribution along the line of sight $C_n^2(z)$ as

$$B(b) = \int_0^\infty W(z, b) C_n^2(z) dz. \quad (1)$$

Here $W(z, b)$ is the *weighting function* (WF). We study here the scintillometer array with four 1-cm round detectors in a linear configuration with coordinates (0, 10, 13.5, 38) cm, see Fig. 1 (left). Apart from the baseline length b , the WF depends on the baseline orientation, lunar phase, detector size, and turbulence outer scale ($L_0 = 25$ m is assumed here).

In the discrete formulation, we select the logarithmic altitude grid with $N_z = 80$ layers from 1 m to 10 km. The sampling of this grid $z_{i+1}/z_i = 1.12365$ is small enough to capture the details of the weighting and response functions. The turbulence profile is sought as a vector C with N_z elements. The turbulence integrals at each grid point J_i equal the products of the C_i with the grid step Δz_i .

The scintillometer array contains N_b baselines (including the zero baseline) and the measured covariances are represented by a vector B with N_b elements. This vector is related to the TP linearly,

$$B = W'C, \quad (2)$$

where $W'_{i,j} = W_{i,j}\Delta z_i$ is the *interaction matrix*, borrowing this term from adaptive optics.

A simple inversion of Eq. 2 to derive the TP does not work, because the number of unknowns is larger than the number of measurements. Some parametrization of the problem is needed to reduce the unknowns to a reasonably small number $N_x \leq N_b$. The vector of *parameters* X can be defined in various ways.

2.2 Linear reconstructor

It is convenient to de-compose the TP on a set of some basis functions T_k ,

$$C_n^2(z) \approx \sum_{k=1}^{N_x} X_k T_k(z). \quad (3)$$

We choose triangular basis functions on the logarithmic distance grid,

$$T_k(z) = 1 - |\log(z/z_k)|/\log(4) \text{ for } |\log(z/z_k)| < \log(4). \quad (4)$$

The central points are $z_k = \{4, 16, 64, 256\}$ m (Fig. 1, right). The first function equals 1 for $z < 4$ m and the last one equals 1 for $z > 256$ m. This set of T_k represents the TP by linear segments between the pivot points z_k and by constants outside this interval. The parameters X_k equal the TP values at the pivot points, $X_k = C_n^2(z_k)$. The matrix T has dimensions $N_z \times N_x$ and interpolates the vector of parameters to all grid points, $C = TX$.

The linear relationship between parameters and measures translates into the matrix equation

$$B = AX, \quad (5)$$

where the elements of the $N_b \times N_x$ interaction matrix A are

$$a_{k,j} = \int W(z, b_j) T_k(z) dz = W'T. \quad (6)$$

The unknown coefficients X can be determined by the standard least-squares (LS) method,

$$X \approx (A^T A)^{-1} A^T B = R_{LS} B. \quad (7)$$

The LS *reconstructor* matrix R_{LS} (dimensions $N_x \times N_b$) translates the measurements B into the unknowns X . The LS reconstructor (7) implicitly assumes that the measurement errors of covariances B are all equal and uncorrelated. In reality the measurements are strongly correlated [6]. However, numerical tests have shown that the optimized reconstructor which takes these errors into account and the simpler LS reconstructor produce comparable results.

2.3 Non-linear reconstructor

Having obtained the first estimate of the TP, X , we now want to refine it by changing slightly the model and using the fact that $C_n^2(z)$ is a non-negative quantity. To do this, we change the parameters to $y = \log C$. The values of y at the pivot points will be the parameters Y of the new model which interpolates y between the pivot points linearly. This corresponds to the approximation of $C_n^2(z)$ by power-law functions between the pivot points. Obviously, $y = TY$ and $C = 10^y$. Putting these reconstructed values into Eq. 2, we obtain the estimate of the covariances \hat{B} . The quality of the restoration can be measured by the closeness between the actual data B and their model \hat{B} , for example as

$$\delta^2 = \frac{1}{N_b B_0^2} \sum_{j=1}^{N_b} (\hat{B}_j - B_j)^2, \quad (8)$$

where B_0 is the covariance at zero baseline (i.e. the scintillation index). The rationale for selecting such simple goodness-of-fit criterion is provided by the analysis of the measurement errors, which are not very different for all elements of the vector B , decreasing only slightly at longer baselines [6]. These errors could be estimated if the TP and wind speed profile were known, but we do not want to complicate the algorithm by invoking these additional parameters. The error metric (8) is thus nearly proportional to the standard χ^2 metric because all measurement errors are proportional to B_0 .

In short, the non-linear method consists in taking the initial parameter estimates Y obtained from the linear reconstruction (we set $Y > -19$ to prevent numerical problems) and minimizing (8). We used initially the Powell routine [2] for the minimization, but found that it fails to converge sometimes, so finally adopted a more robust `amoeba` routine.

The model approximates the TP by segments of power-law functions. Consider some segment between the pivot points z_1 and z_2 , with the fitted C_n^2 values C_1 and C_2 at the ends of this segment. For some value z inside the segment, the model TP is

$$C_n^2(z) = C_1(z/z_1)^a, \quad \text{where } a = \log(C_2/C_1)/\log(z_2/z_1). \quad (9)$$

The integral of this TP from z_1 to z is equal to

$$J(z) = \int_{z_1}^z C_n^2(z) dz = z_1 C_1 [(z/z_1)^{a+1} - 1]/(a+1), \quad (10)$$

where the case $a = -1$ must be considered separately. In practice, we simply interpolate the TP on the whole z =grid and calculate the integrals up to a certain altitude by summation of $C_n^2 \Delta z$.

3 Testing the algorithm

The ability of the algorithm to restore different TPs was tested. The covariances are calculated from the model TP and are presented to the 2-step reconstruction (code `moonx5.pro`). No measurement noise was simulated.

Table 2: TP models (C_0 and C_1 in $10^{-16} \text{ m}^{-2/3}$, h_0 and h_1 in m)

Model	C_0	C_1	h_0	h_1	Figure
2-exponent	50	1	30	10^4	Fig. 2
Power	50	1	20	—	Fig. 3
Gaussian	50	1	10	30	Fig. 4
Top-Hat	50	1	10	30	Fig. 5

3.1 TP models

Several TPs were presented to the reconstruction algorithm (Table 2). The *double-exponential* TP [4] is

$$C_n^2(z) = C_0 \exp(-z/h_0) + C_1 \exp(-z/h_1) \quad (11)$$

with $C_0 = 5 \cdot 10^{-15} \text{ m}^{-2/3}$, $C_1 = 10^{-16} \text{ m}^{-2/3}$, $h_0 = 30 \text{ m}$, and $h_1 = 10 \text{ km}$ (or some variations of these parameters).

The *power-law* TP is

$$C_n^2(z) = C_0(z/h_0)^{-1.5} + C_1 \quad (12)$$

with the same (or similar) constants C_0 and C_1 and $h_0 = 20 \text{ m}$.

The *Gaussian* TP is

$$C_n^2(z) = C_0 \exp[-(z - h_0)^2/(2h_1^2)] + C_1, \quad (13)$$

$h_0 = 10 \text{ m}$, $h_1 = 30 \text{ m}$.

Finally, the *top-hat* TP equals C_0 between h_0 and h_1 and C_1 otherwise, with $h_0 = 20 \text{ m}$ and $h_1 = 30 \text{ m}$.

3.2 Test results

Table 3: Restoration quality (ϵ in percent)

Model	Nominal		Offset		Airmass	
	ϵ_4	ϵ_{200}	ϵ_4	ϵ_{200}	ϵ_4	ϵ_{200}
2-exponent	1	-4	6	1	3	-4
Power	19	4	21	13	32	-4
Gaussian	-4	0	2	10	3	-1
Top-Hat	100	-19	-144	10	13	-1

The results of the TP restoration are presented in Figs. 2,3,4,5. The left-hand panels show the TPs, the right-hand panels plot the cumulative profiles $J(z)$ calculated by summing $C_n^2 \Delta z$ over the grid points, starting from $z = 1 \text{ m}$ upwards. Obviously, the smooth TPs (double-exponential and

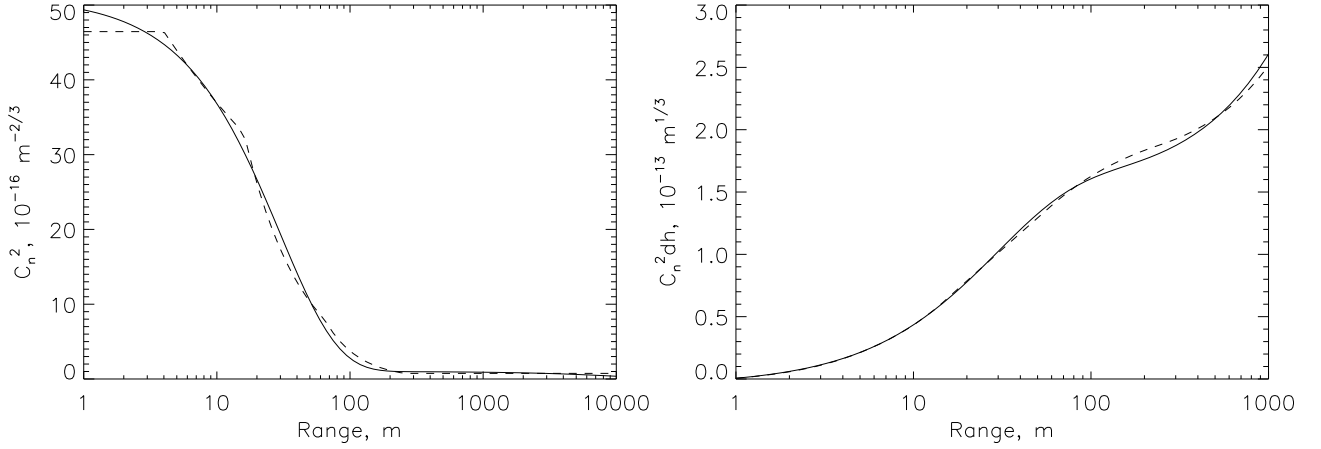


Figure 2: Exponential profile model (full line) and its restoration (dashed line). The cumulative profiles are plotted in the right panel. [profexp,cumexp]

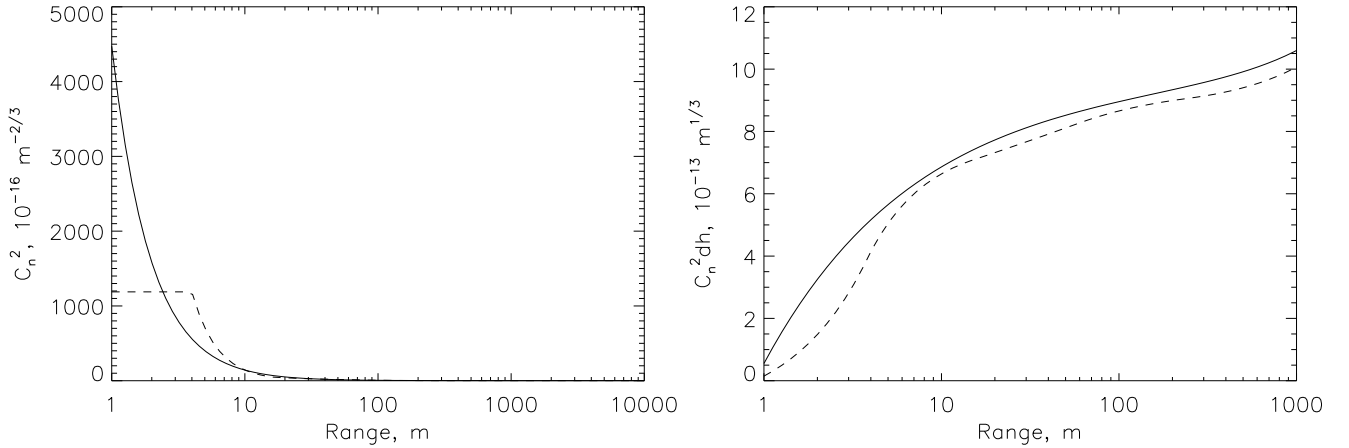


Figure 3: Power-law profile model (full line) and its restoration (dashed line). [profpow,cumpow]

Gaussian) are modeled very well. The errors are larger for the power-law and top-hat models, but even in these cases the restored TPs give a correct indication of the ground-layer seeing and turbulence location.

To quantify the accuracy of the restoration, we define the relative error of the cumulative profiles $\epsilon(z) = (J - J_{\text{rest}})/J$. Of course, we do not expect the restoration to be accurate everywhere, but rather concentrate on the relevant range between 4 m and 200 m. The maximum absolute value of ϵ over this range is a good measure of the accuracy. We found that the relative errors of the cumulative profile at the lowest and highest points, ϵ_4 and ϵ_{200} , are just as representative as ϵ_{max} , because the worst error is usually found at one of the limits. Note that for the top-hat profile, the relative error at the lower limit is large simply because there is very little turbulence below 4 m. The plots show the detailed behavior of the reconstructions.

Relative errors of the cumulative profiles are gathered in Table 3. We did two additional tests. First,

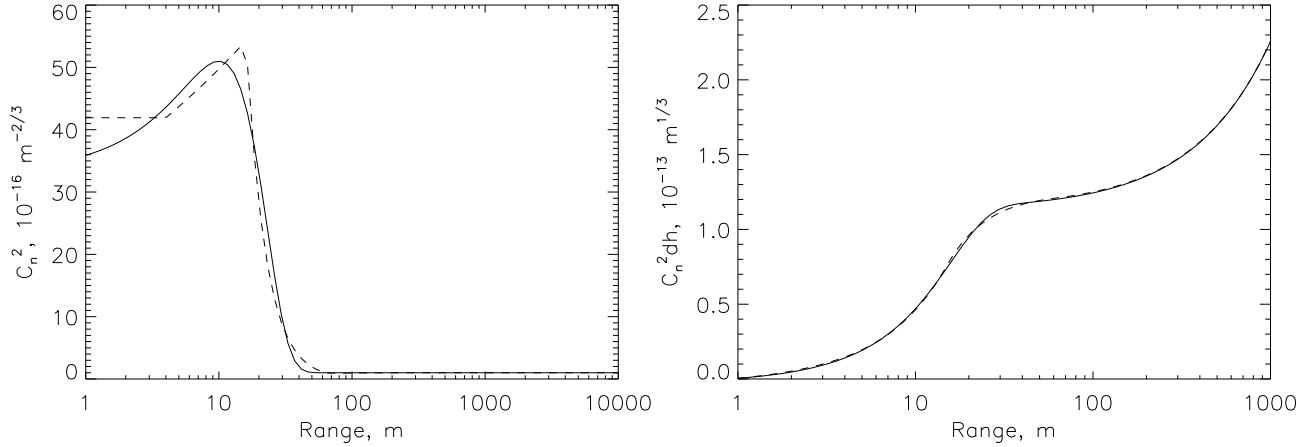


Figure 4: Gaussian profile model (full line) and its restoration (dashed line). [profgauss,cumgauss]

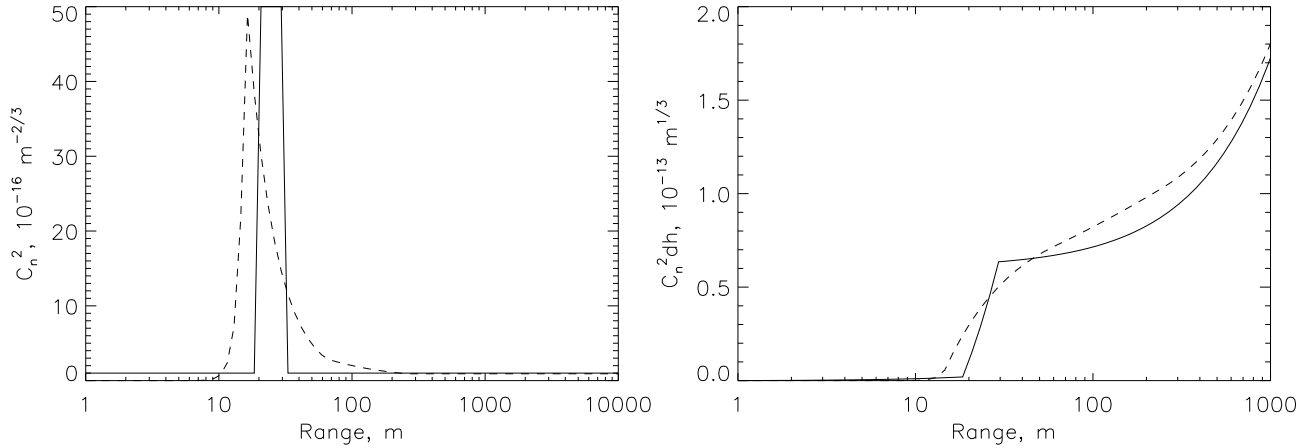


Figure 5: Top-hat profile model (full line) and its restoration (dashed line). [profhat,cumhat]

all covariances were artificially increased by adding 0.5 of the scintillation index. This situation models the effect of high-altitude turbulence which produces slow correlated scintillation at all baselines. Similar bias can be caused by varying atmospheric transmission or by a correlated electrical noise. As expected, the restoration algorithm adjusts by increasing the C_n^2 value at the highest pivot point (256 m), but the results at lower altitudes are affected only mildly. So, the method is robust with respect to the additive bias on covariances.

The second test emulates the effect of observing at an air mass $\sec \gamma = 1.5$ by increasing the altitudes of all pivot points by the same amount. The altitude grid and weighting functions remain unchanged. Again, the results are reasonably accurate. Therefore, we can define the pivot points in altitude (rather than range), which is more convenient for the data interpretation. We also tried to *decrease* the pivot points range and found that the method still works.

3.3 Processing the real data

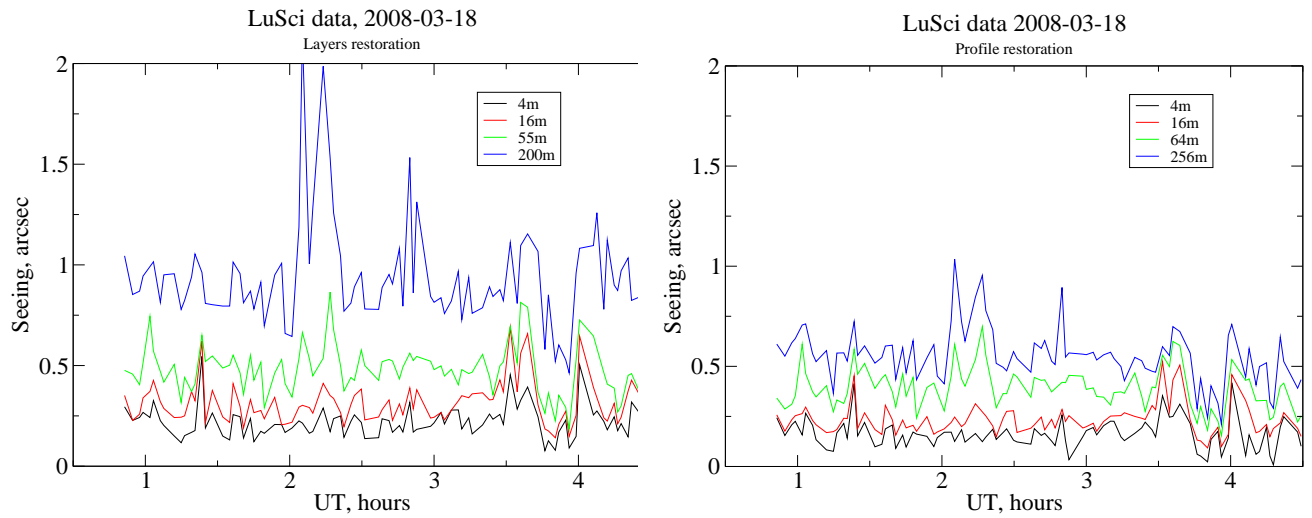


Figure 6: One night of LuSci data at Penyon, March 17/18 2008. Left – “layers” restoration, right – “profile” restoration. [080318layers.eps,080318prof.eps]

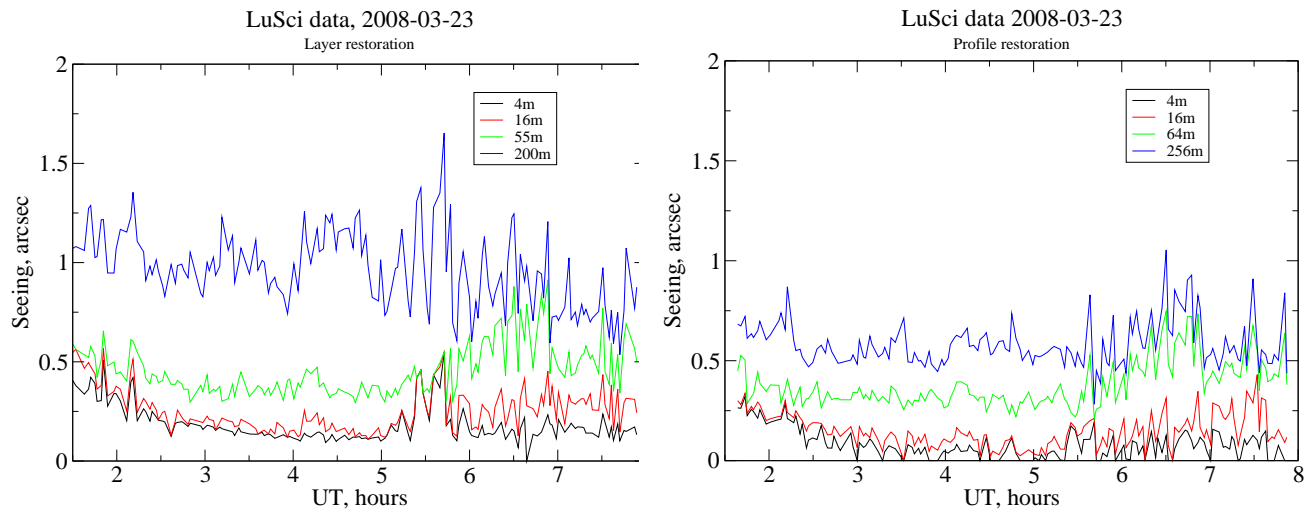


Figure 7: One night of LuSci data at Penyon, March 22/23 2008. Left – “layers” restoration, right – “profile” restoration. [080323layers.eps,080323prof.eps]

A code `profrest.pro` implements the new algorithm. It has been applied to four nights of LuSci data collected at Penyon in March 2008 during the LSST campaign. Figures 6 and 7 show the plots of the same data processed by the old “layers” method and by the new profile-reconstruction method. In the left-hand plots, the numbers indicate mid-points of the layers along the line of sight (i.e. without accounting for the air mass), the upper limits of these layers are rather fuzzy and extend to at least

twice the mid-point. The 200-m layer is particularly ill-defined, its response is simply equal to the weighting function at the longest baseline (Fig. 1) and extends to high altitudes. Moreover, it can be biased by the transparency variations. In contrast, the numbers in the right-hand plots are the upper limits in altitude to which the restored profile has been integrated (the lower limit is ~ 1 m), the corresponding seeing values are fully corrected for the air-mass effect.

The 256-m seeing deduced with the new code is comparable to the sum of the first three layers (55-m seeing). The layers method shows a larger total GL seeing because its response extends to higher altitudes and because it is not corrected for the air mass.

The product of `profrest.pro` is a multi-column file with `.tp` extension. Each line contains the name of the input data file, Julian day, air mass, and the total (256-m) GL seeing in arcseconds. The following 4 numbers are the turbulence integrals (in $\text{m}^{1/3}$) from the ground to the pivot points which are at 4, 16, 64, and 256 m altitudes from the ground. The last 4 numbers are the decimal logarithms of the C_n^2 values (in $\text{m}^{-2.3}$) at the pivot points. Using these 4 numbers, we can calculate the turbulence integrals between any altitudes, as explained above.

4 Conclusions

The proposed restoration method seems to work well. The errors of representing real TPs with a crude model translate to the errors on the turbulence integrals that are mostly below 20%. The error in the measured GL seeing would be 12%. The restoration is robust with respect to the additive errors on all measured covariances. The data product of this algorithm are the four C_n^2 values at pre-defined altitudes of 4, 16, 64, and 256 m and the recipe (10) for calculating turbulence integrals between any altitudes using these four numbers.

References

- [1] Hickson, P. & Lanzetta, K. 2004, *PASP*, 116, 1143
- [2] Press, W.H., Flannery, B.P., Teukolsky, S.A. 1986, *Numerical Recipes: The Art of Scientific Computing* (Cambridge Univ. Press)
- [3] Socas-Navarro, H., Beckers, J., Brandt, P. et al. 2005, *PASP*, 117, 1296
- [4] Tokovinin, A. & Travouillon, T. 2006, *MNRAS*, 365, 1235
- [5] Tokovinin A. Restoration of turbulence profile from lunar scintillation. January 22, 2007. <http://www.ctio.noao.edu/~atokovin/profiler/restoration.pdf>
- [6] Tokovinin A. Random measurement errors in LuSci. February 12, 2008 <http://www.ctio.noao.edu/~atokovin/profiler/errcalc.pdf>